Higher-order mode substrate integrated waveguide cavity excitation for microstrip patch antenna arrays at 30-GHz

View the article online for updates and enhancements.

Journal of Physics Communications

PAPER

Higher-order mode substrate integrated waveguide cavity excitation for microstrip patch antenna arrays at 30-GHz

Bilal T Malik[1] , Viktor Doychinov[1] , Syed Ali R Zaidi[1], Nutapong Somjit[1] , Ian D Robertson[1] and Charles W Turner[2]

[1] School of Electronic & Electrical Engineering, University of Leeds, Leeds, United Kingdom
[2] Department of Informatics, King's College London, London, United Kingdom

E-mail: elbtm@leeds.ac.uk

Abstract

This paper presents a novel approach to the design and fabrication of low-cost and high-gain aperture-coupled microstrip patch antenna (AC-MPA) arrays with improved radiation pattern for millimetre-wave applications such as simultaneous wireless information and power transfer (SWIPT) and Internet-of-Things (IoT) device connectivity. A higher-order mode substrate integrated waveguide (SIW) cavity is used to feed the MPA arrays through aperture coupling. The improved design approach is introduced and discussed in detail. Simulation and experimental results for 2×2 and 4×4 arrays are presented, demonstrating excellent agreement. Key performance metrics are side-lobe levels of less than -24 dB and -29 dB in the E-plane and -22 dB and -26 dB in the H-plane and realized gain of 11 dBi and 15 dBi for the 2×2 and 4×4 arrays respectively, at a design frequency of 30 GHz.

1. Introduction

Substrate integrated waveguide (SIW) technology has demonstrated certain advantages in its use in modern wireless communication systems [1–3]. SIW technology has been used extensively for the design of millimetre-wave antenna arrays, with SIW cavity-backed aperture-coupled microstrip patch antenna (AC-MPA) arrays having gained considerable attraction [4–7]. In this type of antenna array design, the benefits of MPAs are combined with the advantages of SIW technology [5, 6]. Additionally, aperture coupling has been demonstrated to offer higher radiation efficiency, lower return loss and less complexity as compared to other array feeding techniques such as microstrip and coplanar waveguide (CPW) transmission lines [8]. The drawbacks of a microstrip feed network include undesired back-lobe radiation and high insertion loss at millimetre-wave frequencies, which can significantly degrade the radiation pattern and efficiency of the antenna arrays [8].

Recent years have also seen an increase in research into methods to improve antenna performance using metamaterials, periodic structures and 2D materials. Metamaterials, being artificial composite materials, offer the opportunity to make use of refraction properties not found in regular materials, including the well-known negative index and left-handed behavior. For antennas, metamaterials have been shown to offer the potential for miniaturization and control of radiation properties, including loading antenna arrays with metasurfaces [9], while split-ring resonator (SRR) arrays and other metamaterials have been demonstrated for antenna improvement [10]. Furthermore, tunable and reconfigurable metamaterials have been shown to offer exciting new opportunities for spatial electromagnetic wave processing in a range of photonic, terahertz and microwave applications [11]. Other important and related techniques include the use of nanoparticles [12] and 2D materials, especially graphene [13], which have given the fields of plasmonics and transformation optics a new impetus thanks to the control that these materials give over permittivity and permeability, without the ohmic losses associated with conventional conductors. For example, near-zero index materials have been shown to have important advantages for new waveguide structures, including dielectric rod waveguides that can

overcome many of the disadvantages of the dominant microwave and millimeter-wave metallic waveguides, such as their narrow bandwidth, high loss and dispersion [14].

These technologies have a wide range of applications in antennas, for gain and directivity enhancement, mutual coupling reduction and miniaturization [15–17]. In microstrip patch antenna arrays a key role of these techniques is to suppress the surface waves, which results in the gain enhancement and also reduction of side & back lobes, improving the radiation pattern. Near zero index materials can be used to make directive radiation towards the broadside to a planar interface [18]. In [19] the author presented the use of a metamaterial to concentrate the energy radiated by a source in a narrow cone. A high-directivity 5G antenna with near-zero refractive index metamaterial is presented in [17]. The gain of the antenna is improved by more than 6 dBi at $27 \sim 29$ GHz based on the near-zero refractive index metamaterial. A graphene-based circular patch antenna was proposed for 6.8–7.2 THz. Polyimide, quartz, silicon dioxide and silicon nitride were used as substrate materials and evaluated the performance of the patch antenna for individual substrate materials [16]. In a recent publication, microfluidics was used to reconfigure the polarization of antennas when a conductive liquid is injected into the substrate dielectric material [20]. Despite the many advantages of using the above mentioned technologies, the design and manufacture are complex and difficult as compared to the design approach proposed in this paper to enhance the radiation performance and directivity with very low side lobe levels by using a combination of dielectric materials to synchronize the aperture coupling from a higher order mode SIW cavity to the patch antenna array.

In [21], the design of a higher-order mode cavity-backed helical antenna array was proposed. The authors used a TE707 mode resonant cavity to couple power to a 16 element helical antenna array at a center frequency of 11.8 GHz. In [7], a 2×4 patch antenna array was excited by aperture coupled longitudinal slots located in the SIW, at a center frequency of 24 GHz. This antenna had a measured gain of 12.5 dBi, a radiation efficiency of 62% and 3.35% bandwidth for a return loss (RL) level of 10 dB. In recent research papers [22–24], a similar design approach has been used to design SIW cavity-backed aperture-coupled antenna arrays using higher-order mode cavity excitation. In these antenna designs, a TE404 resonant mode was used for the excitation of 4×4 antenna arrays. Despite promising results for the maximum realized gain, the reported antenna arrays have high SLLs of around -14 dB.

The main issues addressed in this research work are the distance between two adjacent peaks of the E-field in SIW cavity is equal to one-half guided wavelength ($\lambda_g/2$), which is always less than the one-half free space wavelength ($\lambda_0/2$) due to the relative permittivity ε_r of the dielectric substrate as $\lambda_g = \lambda_0/\sqrt{\varepsilon_r}$. However, according to the literature [25, 26], in order to minimize the side-lobe levels the spacing between array elements should be greater than or equal to one-half free space wavelength ($\lambda_0/2$), which would not be possible if the TE404 mode in SIW cavity was used for the excitation of 4×4 MPA array. The second issue is that the two adjacent peaks of electric field are $180°$ out of phase, therefore the coupling slots have to be offset in order to make them radiate in phase. However, there might be additional issues in distributing power around every slot, which affects the radiation pattern [27].

To overcome these limitations related to higher-order mode SIW cavity excitation, TE303 and TE707 modes are proposed here for the excitation of 2×2 and 4×4 MPA arrays, respectively. Figure 1 presents the simulated *E*-field distribution inside the SIW cavities for the TE303 and TE707 resonant modes, where the '+' and '−' signs denote the positions of maxima and minima, respectively. There are 3×3 and 7×7 standing wave *E*-field peaks distributed for the TE303 and TE707 cavity modes, respectively. In the antenna array design proposed here, only alternate maxima, having the same phase of the *E*-field, were used for the excitation of the MPA elements, through aperture coupling. This eliminates the need to offset the coupling slots and radiating patches to compensate for the $180°$ phase difference of adjacent maxima.

In this paper we present a modified design approach for the excitation of aperture-coupled microstrip patch antenna arrays via higher-order mode SIW cavities. The proposed approach significantly improves the side-lobe levels of antenna arrays and is validated through the design and measurement of 2×2 and 4×4 millimeter-wave microstrip patch antenna arrays fed by a higher-order mode SIW cavity, with a design frequency of 30 GHz. The advantages of this method include low-cost, straightforward design and fabrication, as well as highly directional radiation pattern with lower side-lobe levels. Additionally, the overall size of the final antenna array is reduced as there is no need for large-area power dividers implemented in microstrip or SIW technology. Proposed antenna arrays are well suited for millimetre-waves far field wireless power transfer applications in Internet-of-things (IoT) sensor nodes, sensing & diagnostics and automotive industry. WPT technologies use electromagnetic fields to transmit power through the air. One of the main requirements for an efficient WPT system is a highly directional antenna with low side-lobe levels (SLLs) and high radiation efficiency [28]. Using an antenna with such parameters maximizes the amount of RF power at the receiver, while at the same time minimizes the interference caused to other, non-WPT receivers [29]. Due to its inherently narrowband nature and low profile, this approach is particularly suitable for short-range simultaneous wireless information and power transfer (SWIPT) to IoT devices and radar applications which do not require high data rates [29].

Figure 1. E-field distribution in the SIW cavities at resonance; (a) TE303 mode, (b) TE707 mode.
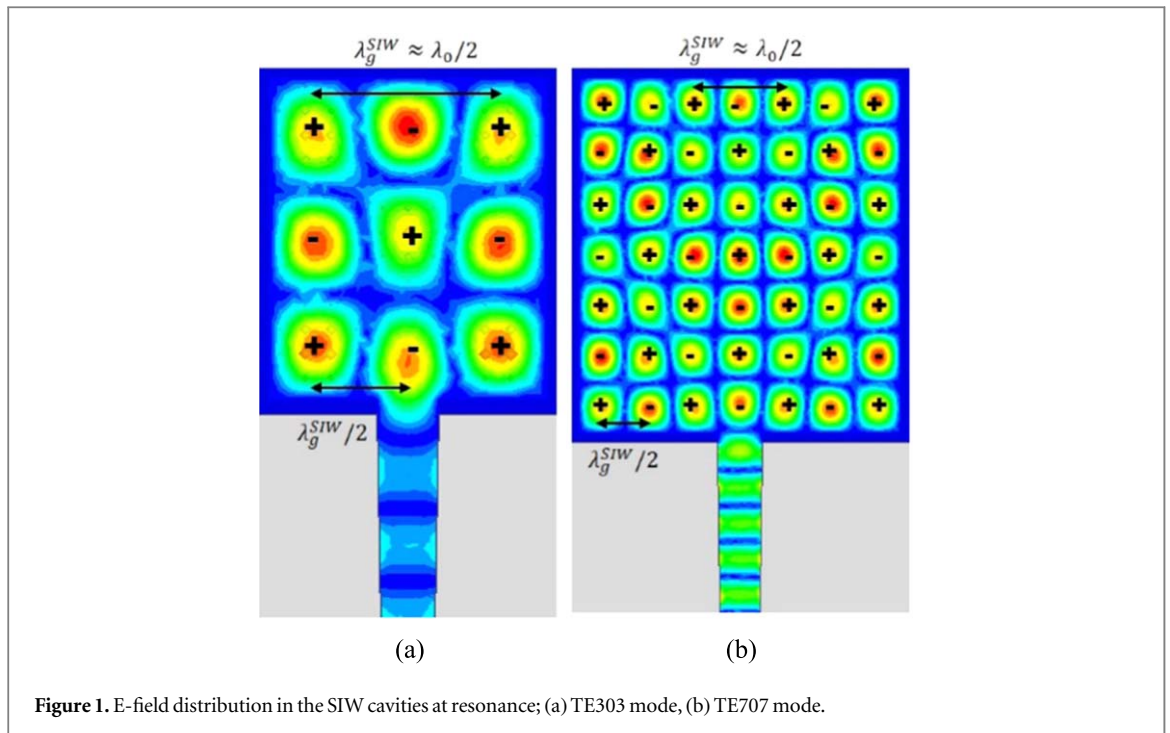
2. Array analysis and design procedure

It is well known that there is a range of electromagnetic modelling techniques that can be applied to microwave, millimeter-wave and terahertz passive components and antennas. Effective medium theory gives a wide range of tools for the analysis of composite materials [30]. The Green's function approach is especially suited to multilayer structures and has been applied to many metamaterial problems, and the technique has recently been extended to analyse surface plasmon resonance at interfaces for metastructures [31]. The absorbing boundary condition method has also been used for metamaterial modelling, such as wideband absorbers using mushroom-type elements [32] and is important for substrate integrated waveguide modelling, which has been demonstrated using the finite-difference frequency domain method [33]. In this research work we used commercially available finite element method (FEM) full-wave electromagnetic solver Ansys HFSS™ to design and analyse the proposed antenna arrays and the proposed structures were fabricated and measured to validate the simulated results.

The general layout of a SIW cavity-backed aperture-coupled MPA array is shown in figure 2. After an extensive literature review on SIW cavity higher-order mode excitation for MPA arrays and a series of simulations and optimization to improve the radiation pattern of antenna arrays using this excitation approach, we identified some drawbacks and limitations of using the TE404 cavity mode for the excitation of a 4×4 MPA array as proposed by [22, 23]./

2.1. Proposed antenna structure

The proposed array configurations consist of a two- layer structure with a higher-order mode SIW resonant cavity in the lower substrate and the microstrip patch antenna array on the top metal surface of the upper substrate. The SIW cavity is fed by a microstrip line on the top surface of the lower substrate. Figures 3 and 4 show the layer stack-up for the 2×2 and 4×4 arrays, respectively.

Transverse coupling slots located on the top metal layer of the SIW substrate allow the resonant cavity to parasitically excite the individual patch antenna array elements. The size and position of these slots determines the coupling between the SIW cavity and the antenna array, while the linear dimensions of the patches determine their operating frequency [8, 27]. It has been shown that a transverse slot excitation provides efficient coupling and higher gain when compared to a longitudinal coupling slot [4]. The proposed approach is straightforward in terms of feed network design, cost effective in terms of fabrication and is expected to give very low side-lobe levels.

2.2. Design methodology

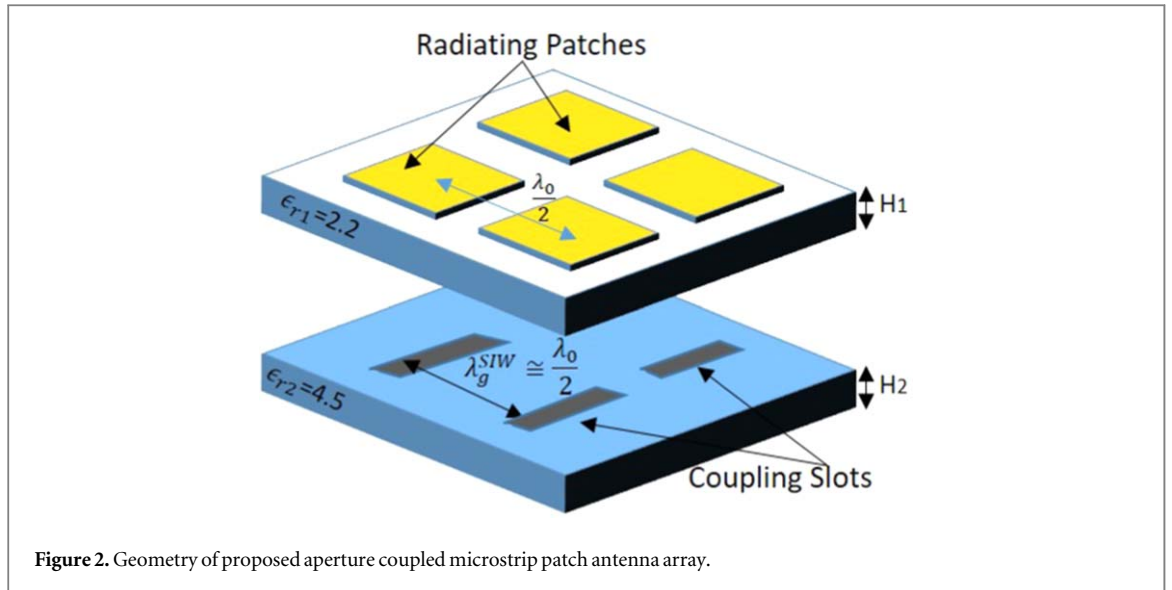The array design methodology that we adopted is as follows:

Figure 2. Geometry of proposed aperture coupled microstrip patch antenna array.
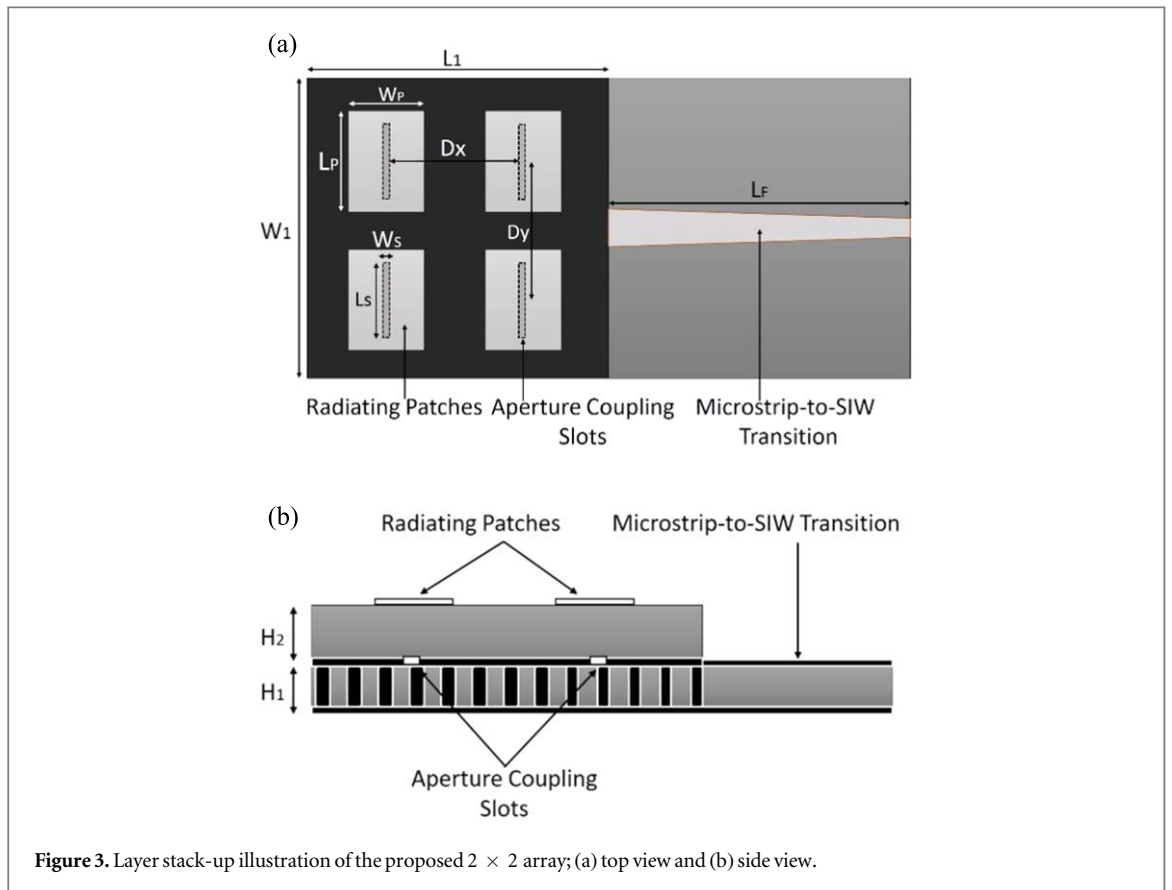

Figure 3. Layer stack-up illustration of the proposed 2 × 2 array; (a) top view and (b) side view.

Step 1) The dimensions of the individual SIW cavities are designed to support the TE303 and TE707 resonant modes at the design frequency of 30 GHz according to [34], which gives the resonant frequency of a TEm0n mode as:

$$f_{m0n} = \frac{c}{2\pi \sqrt{\mu_r \epsilon_r}} \sqrt{\left(\frac{m\pi}{w_{eff}}\right)^2 + \left(\frac{n\pi}{l_{eff}}\right)^2} \tag{1}$$

The effective width and length of the SIW cavity can be calculated using the following equations [17]:
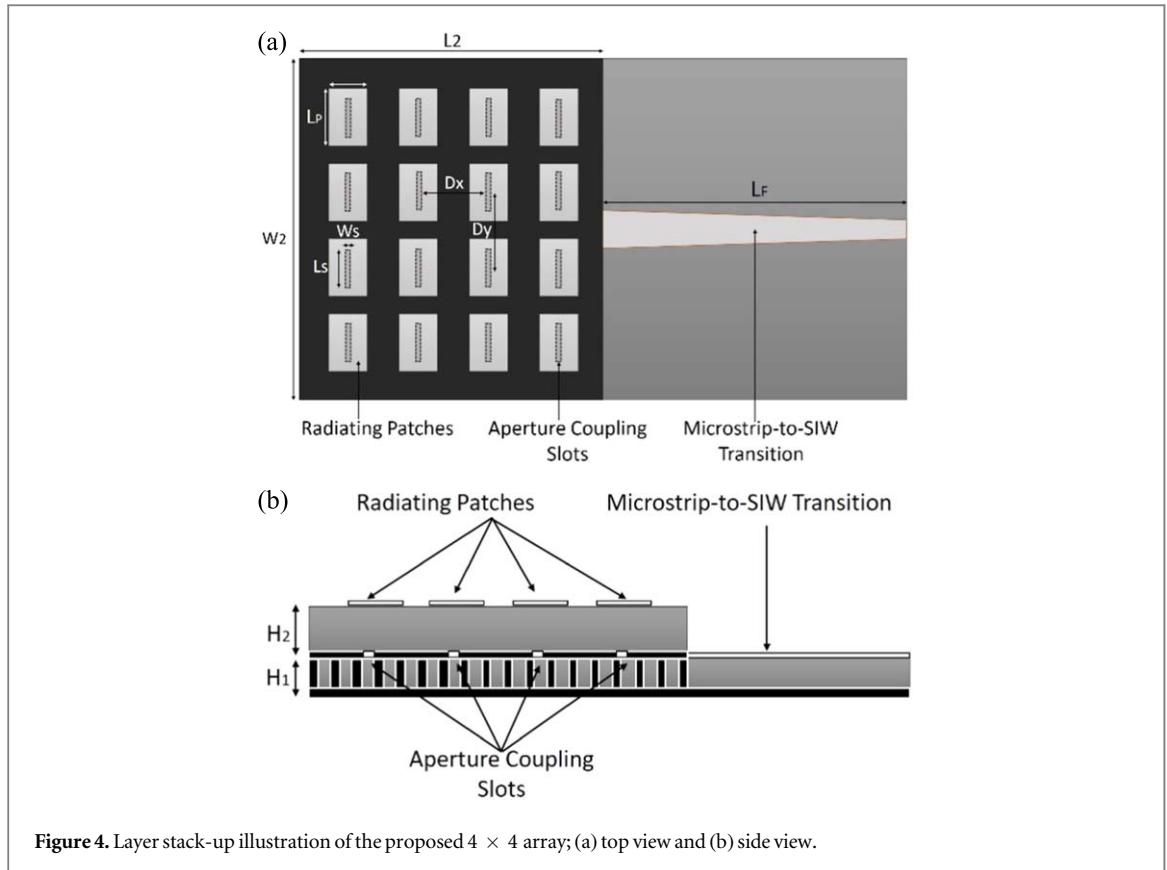
$$w_{eff} = w - \frac{d^2}{0.95p} \tag{2}$$

Figure 4. Layer stack-up illustration of the proposed 4 × 4 array; (a) top view and (b) side view.

$$l_{eff} = l - \frac{d^2}{0.95p} \tag{3}$$

In the above, w_{eff} and l_{eff} are the effective width and length of the SIW cavity, c is the speed of light in vacuum, d is the via hole diameter, p is the distance between two adjacent via holes (centre-to-centre) and is μ_r and ε_r are the relative permeability and permittivity of the substrate material, respectively. To simplify the design, w_{eff} was initially set equal to l_{eff}. The indices m and n had the values 3 and 7 for the TE303 and TE707 modes, respectively.

The diameter of the SIW via holes and the distance between two adjacent ones should be determined according to the following conditions:

$$d < \frac{\lambda_g^{SIW}}{5} \tag{4}$$

$$p < 2d \tag{5}$$

Step 2) The next step is to design the transverse coupling slots in the SIW cavity layer, as well as the 2 × 2 and 4 × 4 MPA arrays on the top metal surface of the upper substrate material, as illustrated in figures 3 and 4. In order to obtain coupling at the desired operating frequency, the physical size of coupling slots and radiating elements are calculated using equations (6)–(12) as reported in [1, 35]. The arrangement of the radiating elements is determined by keeping the distance from the centre of the first slot to the centre of the second slot as $\boldsymbol{\lambda_g^{SIW}} = \frac{\lambda_0}{\sqrt{\epsilon_r}}$ and the distance from the centre of the last slot to SIW end wall as $\boldsymbol{\lambda_g}/2$; As reported in [22, 23], the TEm0n mode coupling level and return loss of the multilayer transition can be controlled by varying the physical slot width, and the physical slot length, while maintaining the slot position at the maximum E-field point. The initial dimensions of coupling slots were determined as follows [35]:

$$l_s = \frac{\lambda_0}{\sqrt{2(\varepsilon_r + 1)}} \tag{6}$$

$$w_s \leqslant \frac{l_s}{10} \tag{7}$$

In this proposed design, one coupling slot per patch element is used, with the slots positioned in the top metal wall of the SIW cavity in such a way as to coincide with a maximum of the *E*-field. The initial dimensions of the MPAs were determined according to well-known equations given below [25]:

The width of the patch is given as:

$$W = \frac{c_o}{2f_r}\sqrt{\frac{2}{\varepsilon_r + 1}} \tag{8}$$

Where c_o is the speed of light in vacuum and f_r is the desired resonant frequency of the antenna.

The effective dielectric constant E_{reff} of substrate is then approximated as:

$$E_{reff} = \frac{\epsilon_r + 1}{2} + \frac{\epsilon_r - 1}{2} + \left[1 + 12\frac{h}{w}\right]^{-\frac{1}{2}} \tag{9}$$

The effective length L_{eff} of the patch is:

$$L_{eff} = \frac{c_o}{2f_r\sqrt{E_{reff}}} \tag{10}$$

The length extension ΔL of the patch due to fringing effect of the E-fields is:

$$\frac{\Delta L}{h} = \frac{(E_{reff} + 0.3)\left(\frac{w}{h} + 0.264\right)}{(E_{reff} + 0.258)\left(\frac{w}{h} + 0.8\right)} \tag{11}$$

Now, the actual Length of the patch is given as:

$$L = L_{eff} - 2\Delta L \tag{12}$$

Step 3) The spacing between the neighbouring array elements is an important parameter which determines the phase difference between the two adjacent array elements and affects the radiation pattern of the antenna array [27]. In order to minimise the side-lobe levels and grating lobes, the centre-to-centre distance between the individual MPA array elements should be $\lambda_0/2$ at the operating frequency of 30 GHz [26]. Therefore, in order to excite all patch elements in-phase, the centre-to-centre distance of the transverse coupling slots should also be $\lambda_0/2$. Since the slots themselves are positioned above neighbouring in-phase maxima of the *E*-field in the SIW cavity, it follows that the guide wavelength in the SIW cavity λ_g^{SIW}, should be equal to one-half the free-space wavelength $\lambda_0/2$. Therefore, the relative permittivity ε_r of the SIW substrate should be selected according to the relation $\lambda_g^{SIW} = \lambda_0/\sqrt{\varepsilon_r}$.

For the designs presented in this paper, Rogers TMM 4 with relative permittivity 4.5 and thickness 0.508 mm was used for the lower (SIW) substrate layer and Rogers RT/Duroid 5880 with relative permittivity 2.2 and thickness 0.787 mm was used for the upper (MPA) substrate layer. As the free space wavelength is 10 mm for a centre frequency of 30 GHz, the $\lambda_0/2$ spacing between the patches should be approximately 5 mm, and the guide wavelength λ_g^{SIW} was calculated to be approximately 5 mm for a substrate with $\varepsilon_r = 4.5$ at 30 GHz.

Step 4) Finally, parametric analysis in HFSS™ was used to find the optimal positions and dimensions of the coupling slots and radiating patches to maximize the coupled power from SIW cavity to MPA array and to minimize the side-lobe levels. The dimensions and position of the coupling slot significantly affect the coupling between the SIW and the microstrip patch, while the dimensions of the patch affect the resonant frequency of the antenna. A tapered microstrip-to-SIW transition is used to feed the higher-order mode SIW cavity. The length of the microstrip feed line is extended to avoid possible reflections due to the coaxial end-launch connector. The final, optimised values for the dimensions of the proposed AC-MPA arrays are summarized in table 1.

3. Results and discussion

The two arrays shown in figure 5 were fabricated and measured using the in-house facilities at the University of Leeds. Several samples for both the 2 × 2 and 4 × 4 variants were fabricated and tested, the measured results are presented here.
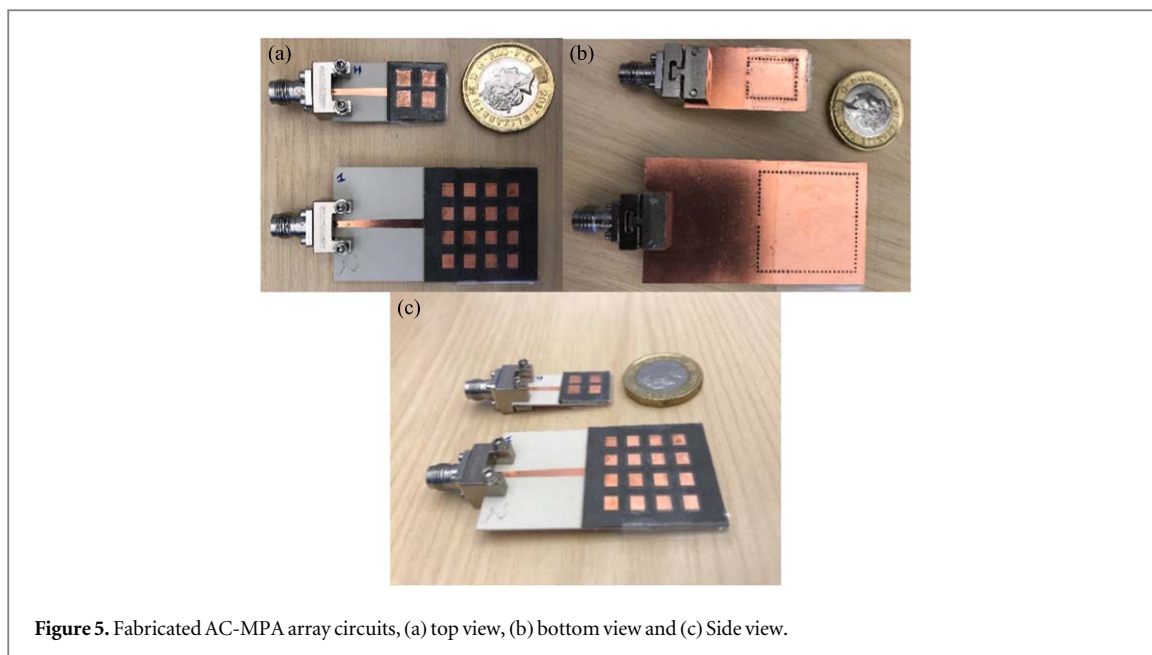
Figure 5. Fabricated AC-MPA array circuits, (a) top view, (b) bottom view and (c) Side view.
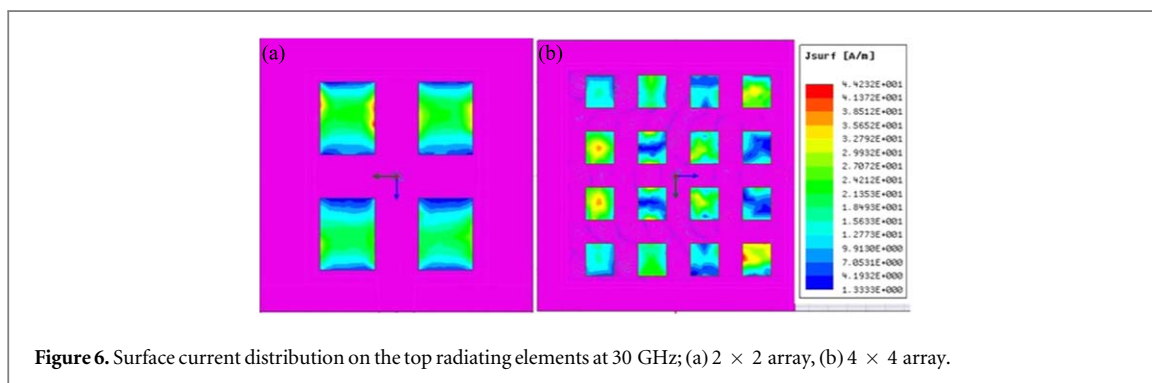

Figure 6. Surface current distribution on the top radiating elements at 30 GHz; (a) 2 × 2 array, (b) 4 × 4 array.

**Table 1.** Final design parameter values.

Parameter	Value (mm)	Parameter	Value (mm)
L_1	12.0	L_S	3.25
W_1	11.5	W_S	0.25
L_2	25.0	L_P	3.0
W_2	25.0	W_P	3.5
H_1	0.51	D_X	5.5
H_2	0.787	D_Y	6.0

The return loss performance of the antennas was measured in laboratory conditions using a Keysight N5247A PNA-X with 1-port Short, Open, Load (SOL) calibration, bringing the S-parameter reference plane to the end of the coaxial cable used. The E-plane and H-plane radiation patterns were measured in a far-field anechoic chamber using a Keysight E8361C PNA and a 20 dBi WR-28 standard gain horn antenna.

To analyse the electromagnetic properties of the structures and the effects of surface waves, the finite element method (FEM) is used to simulate their performance. The effects of surface wave excitation are lower antenna efficiency, degradation of the radiation pattern and undesired coupling between the elements in an array design [36, 37]. The reflection coefficient and the radiation efficiency of proposed antennas clearly shows the minimum effect of surface wave propagation in proposed design. Surface currents distribution on top radiating patches of proposed antenna arrays are shown in figure 6 which shows minimum surface wave propagation and mutual coupling between the arrays elements.

Figure 7. Simulated and measured return loss performance: (a) 2 × 2 array and (b) 4 × 4 array.
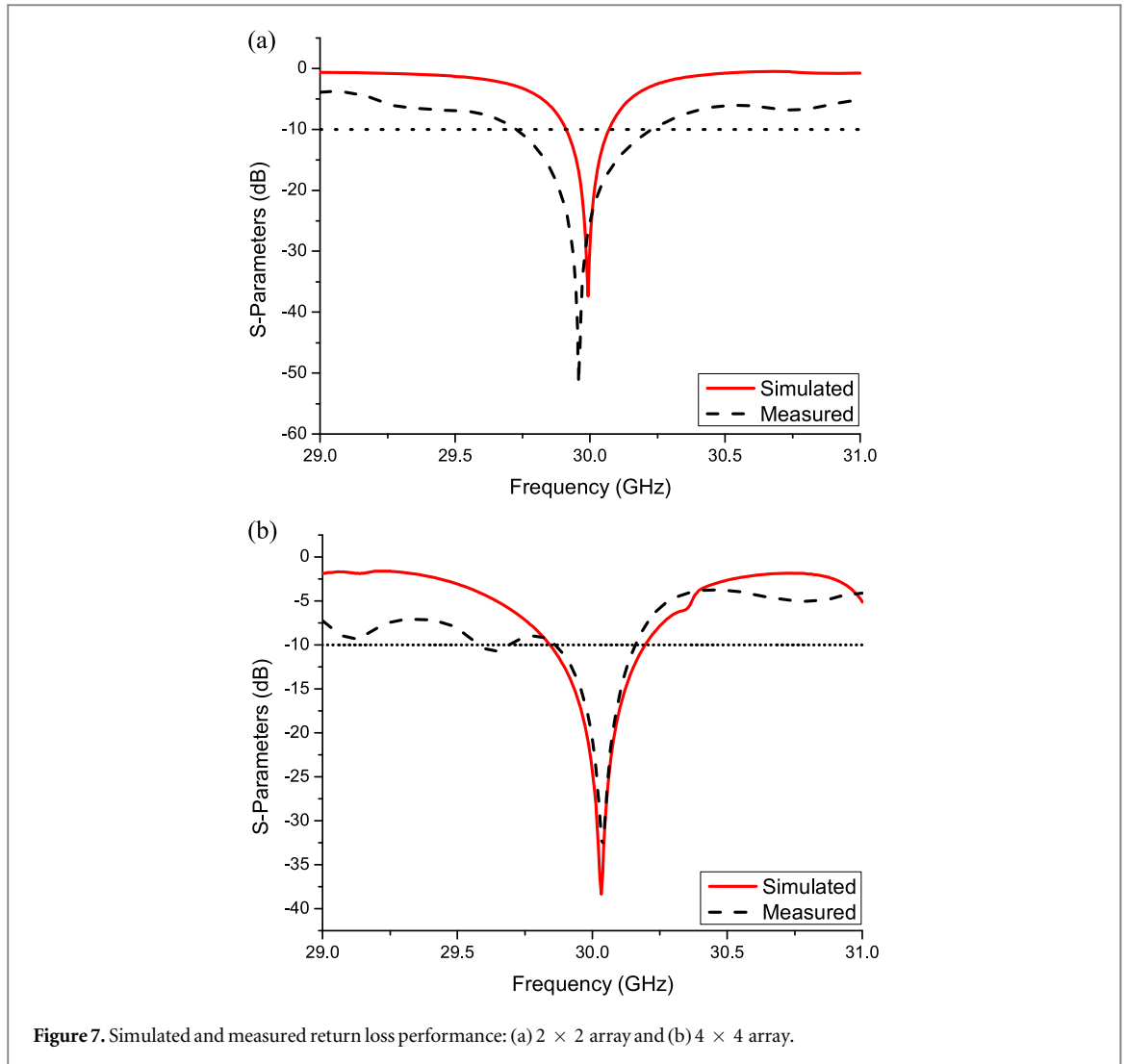
A comparison between the simulated performance in HFSS™ and the measurement results for both the 2 × 2 and 4 × 4 arrays is presented in figure 7. A return loss level of 10 dB is used to define the operating bandwidth of the antennas, found to be 505 MHz for the 2 × 2 array and 300 MHz for the 4 × 4 array. The graphs demonstrate excellent match between simulation and measurement, with minor differences in out-of-band performance. The differences are attributed to the coaxial end-launch connector, as well as higher-than-expected dielectric loss at millimetre-wave frequencies.
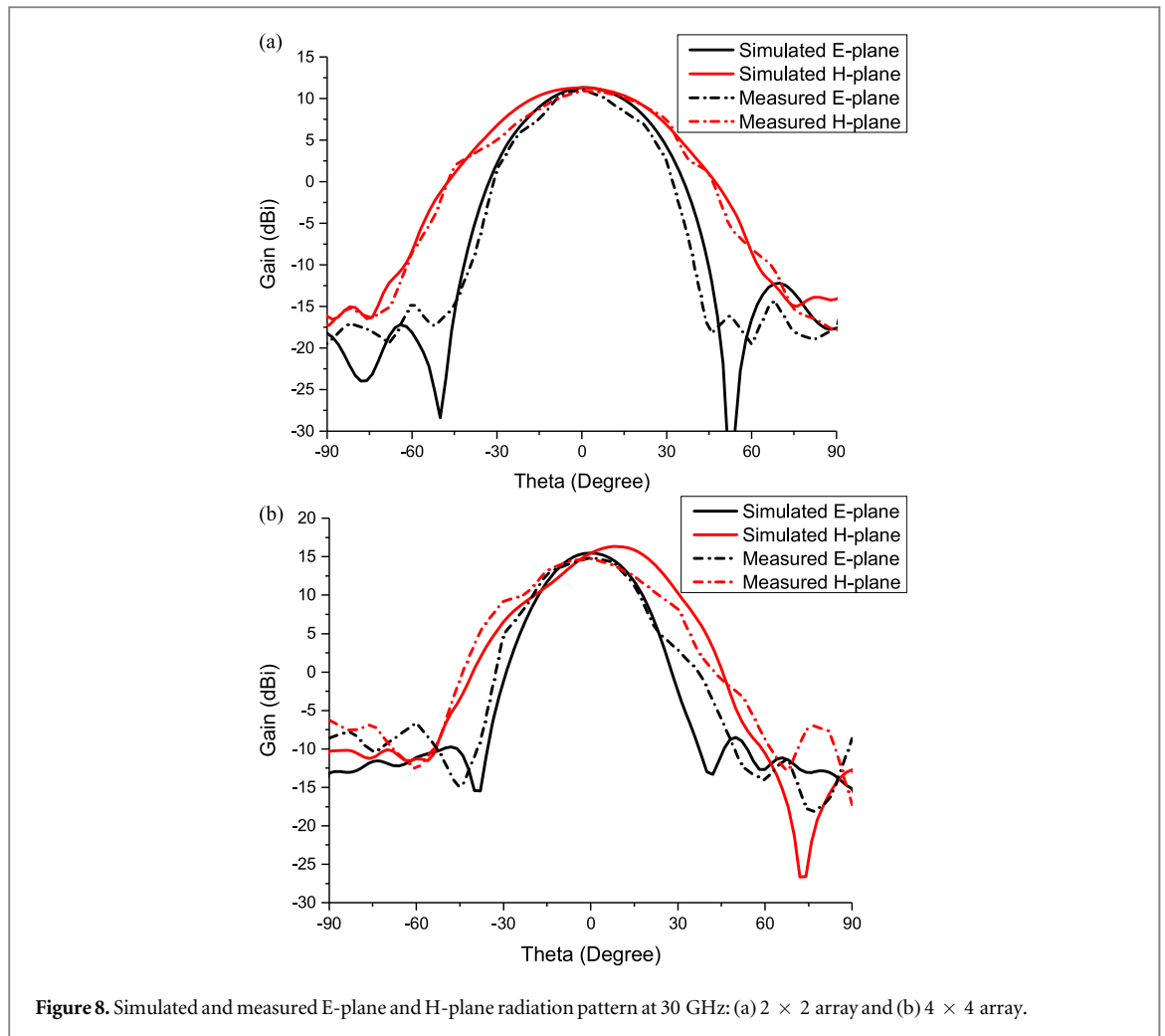
The simulated and measured results for the E-plane and H-plane radiation patterns of the two arrays are shown in figure 8. There is again an excellent qualitative and quantitative agreement between the two, validating the proposed design method, 2 × 2 array provides a maximum gain of 11.1 dBi at the centre frequency of 30 GHz, with SLLs below −24 dB in the E-plane and −22 dB in the H-plane. Full-width at half-maximum (FWHM) for this array is found to be 380/560 in the E/H plane. From figure 8(b), the 4 × 4 array provides a maximum gain of 15 dBi, with SLLs below −29 dB and −26 dB for the E-plane and H-plane, respectively, while the FWHM in this case is 290/380 in the E/H plane. The measured efficiencies of the 2 × 2 and 4 × 4 array are 83.2% and 86.5%, calculated as follows [25]:

$$D \approx \frac{32400}{\theta_{1d} \theta_{2d}} \tag{13}$$

where θ_{1d} & θ_{2d} are the half-power beamwidths in E & H plane (in degrees) respectively.

$$\varepsilon = \frac{G}{D} \tag{14}$$

Where G is the gain and D is the directivity of antenna.

Figure 8. Simulated and measured E-plane and H-plane radiation pattern at 30 GHz: (a) 2 × 2 array and (b) 4 × 4 array.

The obtained results demonstrate the excellent performance of the proposed feeding and excitation approach of higher-order mode SIW cavity backed AC-MPA arrays. While this approach yields inherently narrowband antenna arrays, this is seen as an advantage as the target application is SWIPT for low data-rate IoT devices. Furthermore, these designs can be readily scaled to higher frequencies, potentially enabling SWIPT at the 60 GHz ISM frequency band. Table 2 demonstrates a comparison of results of proposed antenna arrays with other similar antenna designs in the open literature.

4. Conclusion

In this paper, a new approach for the design of AC-MPA arrays fed by a higher-order mode SIW cavity is presented and validated through measurement results of 2 × 2 and 4 × 4 arrays. The proposed arrays are straightforward to design and cost-effective to fabricate. The measurement results show excellent agreement with simulated ones. The arrays exhibit extremely low side-lobe levels in both the E-plane and the H-plane as compared to recent published work, summarised in table 2, with high gains.

The proposed antenna arrays have highly directional radiation pattern with high gain, and low side lobe levels which makes them a promising candidate for high frequency wireless power transfer to IoT sensor nodes. However, due to their narrowband nature, they would not be suitable for high data rate applications, such as fifth generation mobile communications (5G).

Future developments will see the same design approach used to implement larger arrays of 8 × 8 and 16 × 16 elements, as well as at higher frequency bands such as 60 GHz as well. Additionally, the bandwidth can be improved using enhancement techniques discussed previously. Finally, a practical demonstrator for wirelessly powered IoT sensor node will be presented in a future work.

Table 2. Comparison of proposed design approach with recent published work in open literature.

| References | Freq. (GHz) | Size (mm) | Gain (dBi) | SLLs (dB) | | Eff. % | Antenna type | SIW cavity mode | Design complexity |
				E-Pl.	H-Pl.				
[23]	5.8	$2.11\,\lambda_o \times 2.11\lambda_o \times 0.18\lambda_o$	12.9	-14	-15	—	Slot Antenna	TE404	High
[22]	28	$2.33\lambda_o \times 2.33\lambda_o \times 0.19\lambda_o$	15.5	-14	-16	96 (Sim)	Slot Antenna	TE404	High
[21]	11.8	$5\lambda_o \times 5\lambda_o \times 0.19\lambda_o$	$15 \sim 20$	—	—	50	Helical	TE707	High
[7]	24	$4.8\lambda_o \times 1.28\lambda_o \times 0.13\lambda_o$	12.5	-20	-15	62	MPA	TE104	High
[24]	5.8	$1.68\lambda_o \times 1.68\lambda_o \times 0.17\lambda_o$	13.5	-22	-12	91	Slot Antenna	TE303	High
Proposed 4×4	30	$2.5\lambda_o \times 3\lambda_o \times 0.13\lambda_o$	15	-29	-26	86.5	MPA	TE707	Low
Proposed 2×2	30	$1.2\lambda_o \times 1.6\lambda_o \times 0.13\lambda_o$	11.1	-24	-22	83.2	MPA	TE303	Low

Acknowledgments

ORCID iDs

Bilal T Malik ⓘ https://orcid.org/0000-0003-2832-531X
Viktor Doychinov ⓘ https://orcid.org/0000-0001-6730-0057
Nutapong Somjit ⓘ https://orcid.org/0000-0003-1981-2618

References

[1] Moitra S, Mukhopadhyay A K and Bhattacharjee A K 2013 Ku-band substrate integrated waveguide (SIW) slot array antenna for next generation networks *Global Journal of Computer Science and Technology* **13** 11–16 https://globaljournals.org/item/1605-ku-band-substrate-integrated-waveguide-siw-slot-array-antenna-for-next-generation-networks

[2] Yan L *et al* 2004 Simulation and experiment on SIW slot array antennas *IEEE Microwave and Wireless Components Letters* **14** 446–8

[3] Yang Q-L *et al* 2016 SIW multibeam array for 5G mobile devices *IEEE Access* **4** 2788–96

[4] Abdel-Wahab W M and Safavi-Naeini S 2011 Wide-bandwidth 60-GHz aperture-coupled microstrip patch antennas (MPAs) fed by substrate integrated waveguide (SIW) *IEEE Antennas and Wireless Propagation Letters* **10** 1003–5

[5] Awida M H, Suleiman S H and Fathy A E 2010 Development of a substrate-integrated Ku-band cavity-backed microstrip patch sub-array of dual linear/circular polarization for DBS applications *Radio and Wireless Symposium (RWS), IEEE. 2010 (Piscataway, NJ)* (IEEE) (https://doi.org/10.1109/RWS.2010.5434210)

[6] Awida M H, Suleiman S H and Fathy A E 2011 Substrate-integrated cavity-backed patch arrays: a low-cost approach for bandwidth enhancement *IEEE Trans. Antennas Propag.* **59** 1155–63

[7] Rossello J *et al* 2014 Substrate integrated waveguide aperture coupled patch antenna array for 24 GHz wireless backhaul and radar applications *Antenna Measurements & Applications (CAMA), IEEE Conference on. 2014 (Piscataway, NJ)* (IEEE) (https://doi.org/10.1109/CAMA.2014.7003408)

[8] Mikulasek T and Lacik J 2014 Two feeding methods based on substrate integrated waveguide for microstrip patch antennas *IET Microwaves, Antennas & Propagation* **9** 423–30

[9] Dong Y and Itoh T 2012 Metamaterial-based antennas *Proc. IEEE* **100** 2271–85

[10] Rani R, Kaur P and Verma N 2015 Metamaterials and their applications in patch antenna: a review *International Journal of Hybrid Information Technology* **8** 199–212

[11] Zheludev N I and Kivshar Y S 2012 From metamaterials to metadevices *Nat. Mater.* **11** 917

[12] La Spada L and Vegni L 2018 Electromagnetic nanoparticles for sensing and medical diagnostic applications *Materials* **11** 603

[13] Vakil A and Engheta N 2011 Transformation optics using graphene *Science* **332** 1291–4

[14] La Spada L and Vegni L 2017 Near-zero-index wires *Opt. Express* **25** 23699–708

[15] Adel B and Ahmed A 2016 Metamaterial enhances micro strip antenna gain *Microwaves RF* **7** 46–50

[16] Azam S *et al* 2017 Graphene based circular patch terahertz antenna using novel substrate materials *6th International Conference on Informatics, Electronics and Vision & 2017 7th International Symposium in Computational Medical and Health Technology (ICIEV-ISCMHT). 2017 (Piscataway, NJ)* (IEEE) (https://doi.org/10.1109/ICIEV.2017.8338605)

[17] Jiang H *et al* 2018 A high gain 5G antenna with near zero refractive index superstrate *2018 International Conference on Microwave and Millimeter Wave Technology (ICMMT) (Piscataway, NJ)* (IEEE) (https://doi.org/10.1109/ICMMT.2018.8563494)

[18] Silveirinha M G *et al* 2008 Overview of theory and applications of epsilon-near-zero materials *URSI General Assembly* (Citeseer)

[19] Enoch S *et al* 2002 A metamaterial for directive emission *Phys. Rev. Lett.* **89** 213902

[20] Naqvi A H and Lim S 2018 Microfluidically polarization-switchable metasurfaced antenna *IEEE Antennas and Wireless Propagation Letters* **17** 2255–9

[21] Chana S and Turner C 1993 Computer aided design of an overmoded cavity-backed helical antenna array *Electron. Lett.* **29** 1378–80

[22] Asaadi M and Sebak A 2017 High-gain low-profile circularly polarized slotted SIW cavity antenna for MMW applications *IEEE Antennas and Wireless Propagation Letters* **16** 752–5

[23] Han W *et al* 2016 Single-fed low-profile high-gain circularly polarized slotted cavity antenna using a high-order mode *IEEE Antennas and Wireless Propagation Letters* **15** 110–3

[24] Han W *et al* 2015 Single-fed high-gain circularly polarized slotted cavity antenna using TE 330 mode *International Symposium on Antennas and Propagation (Piscataway, NJ)* (IEEE) (https://doi.org/10.1109/APS.2015.7304725)

[25] Johnson R C and Jasik H 1984 *Antenna Engineering Handbook* (New York: McGraw-Hill Book Company) 1356

[26] Mailloux R J 2005 *Phased Array Antenna Handbook* Vol 2 (Boston: Artech House) 9781580536899

[27] Abdel-Wahab W M, Busuioc D and Safavi-Naeini S 2011 Millimeter-wave high radiation efficiency planar waveguide series-fed dielectric resonator antenna (DRA) array: analysis, design, and measurements *IEEE Trans. Antennas Propag.* **59** 2834–43

[28] Mehrotra R 2014 *Cut the Cord: Wireless Power Transfer, its Applications, and its Limits. CSE. Wustl. Edu* 1–11 https://www.cse.wustl.edu/~jain/cse574-14/ftp/power.pdf

[29] Massa A *et al* 2013 Array designs for long-distance wireless power transmission: state-of-the-art and innovative solutions *Proc. IEEE* **101** 1464–81

[30] Sihvola A H 1999 (Electromagnetic Mixing Formulas and Applications: Iet.) (London: IET Digital Library) (https://doi.org/10.1049/PBEW047E)

[31] La Spada L, Tarparelli R and Vegni L 2014 Spectral green's function for SPR meta-structures *Mater. Sci. Forum* (https://doi.org/https://doi.org/10.4028/www.scientific.net/MSF.792.110)

[32] Padooru Y R *et al* 2012 New absorbing boundary conditions and analytical model for multilayered mushroom-type metamaterials: applications to wideband absorbers *IEEE Trans. Antennas Propag.* **60** 5727–42

[33] Xu F *et al* 2003 Finite-difference frequency-domain algorithm for modeling guided-wave properties of substrate integrated waveguide *IEEE Trans. Microw. Theory Tech.* **51** 2221–7

[34] Kumar H, Jadhav R and Ranade S 2012 A review on substrate integrated waveguide and its microstrip interconnect *Journal of Electronics and Communication Engineering* **3** 36–40

[35] Aftanasar M and Hafiz M 2016 Fabricated multilayer SIW system using PCB manufacturing process *Applied Electromagnetics (APACE), IEEE Asia-Pacific Conference on. 2016 (Piscataway, NJ)* (IEEE) (https://doi.org/10.1109/APACE.2016.7915861)

[36] Komanduri V R *et al* 2013 A general method for designing reduced surface wave microstrip antennas *IEEE Trans. Antennas Propag.* **61** 2887–94

[37] La Spada L, Haq S and Hao Y 2017 Modeling and design for electromagnetic surface wave devices *Radio Sci.* **52** 1049–57